JPET # 257097

Title Page

Cellular Vesicles: New insights in engineering methods, interaction with cells and potential for brain targeting

A. Marazioti[1], K. Papadia[2], M.Kannavou[1,2], M. Spella[3], A. Basta[1,2], A-L de Lastic[4], M . Rodi[4], A. Mouzaki[4], M. Samiotaki[5], G. Panayotou[5], G.T. Stathopoulos[3, 6], S.G. Antimisiaris[1,2,]

[1] Foundation for Research and Technology Hellas, Institute of Chemical Engineering Sciences, FORTH/ICE-HT, Rio 26504, Greece

[2] Laboratory of Pharmaceutical Technology, Department of Pharmacy, University of Patras, Rio 26510, Greece

[3] Laboratory for Molecular Respiratory Carcinogenesis, Department of Physiology, Faculty of Medicine, University of Patras, Rio 26510, Greece

[4] Laboratory of Immunohematology, Division of Hematology, Department of Internal Medicine, Medical School, University of Patras, Patras, Greece

[5] B.S.R.C. Alexander Fleming, 16672 Vari, Attica, Greece.

[6] Comprehensive Pneumology Center (CPC) and Institute for Lung Biology and Disease (iLBD), University Hospital, Ludwig-Maximilians University and Helmholtz Center Munich, Member of the German Center for Lung Research (DZL); Max-Lebsche-Platz 31, 81377 Munich, Bavaria, Germany

KEYWORDS: exosomes, extracellular, cellular, vesicles, liposomes, targeting, endothelial, blood brain barrier,

1

Running Title page

Running title: New insights in Cellular Vesicles for Drug Delivery

*Corresponding author

Sophia G. Antimisiaris*

Laboratory of Pharmaceutical Technology, Department of Pharmacy, University of Patras &

Foundation for Research and Technology Hellas, Institute of Chemical Engineering Sciences,

FORTH/ICE-HT, Rio 26504, Greece. Email ID: santimis@upatras.gr, Phone Number: +32610962332

Number of text pages: 22

Number of tables: 4

Number of figures: 8

Number of references: 54

Number of words in abstract: 192

Number of words in introduction: 608

Number of words in discussion: 1388

Supplemental data: Figure S.1, S.2, S.3, S.4, S.5; Table S.1, S.2

Abbreviations: B16: C57BL/6 mouse B16F10 skin melanoma cells; Chol: cholesterol; CVs: Cellular

Vesicles; DiR: 1,1-dioctadecyl-3,3,3,3-tetramethylindotricarbocyanine iodide; DLS: Dynamic light

scattering ; FI :Fluorescence intensity; FITC: Fluorescein-isothiocyanate-dextran-4000; FVB (Friend

leukemia virus B); hCMEC/D3: Immortalized human cerebral microvascular endothelial cells; HEK:

Human HEK-293 embryonic kidney cells; LIP: Liposomes LY: Lucifer yellow-CH dilithium salt;

OX-26: Mouse anti-rat CD71 IgG2a; PC: 1,2-distearoyl-sn-glycerol-3-phosphatidylcholine; PEG: 1,2-

distearoyl-sn-glycerol-3-phosphoethanolamine-N-[methoxy(polyethyleneglycol)-2000]; PEG-MAL:

1,2-distearoyl-sn-glycero-3-phosphoethanolamine-N-[maleimide(polyethylene glycol)-2000] ; PG:

2

1,2-distearoyl-sn-glycero-3-phospho-(1'-rac-glycerol) (sodium salt); RHO: lissamine rhodamine B

phosphatidylethanolamine; TEER: Trans-Endothelial electrical resistance; t-LIP: Targeted liposomes

Recommended section:Special section **Drug delivery and translational medicine**

1,2-distearoyl-sn-glycero-3-phospho-(1'-rac-glycerol) (sodium salt); RHO: lissamine rhodamine B

phosphatidylethanolamine; TEER: Trans-Endothelial electrical resistance; t-LIP: Targeted liposomes

Abstract

Cellular vesicles (CVs) have been proposed as alternatives to exosomes for targeted drug delivery. CVs, prepared from HEK-293, B16F10 and hCMEC/D3 cells, by liposome technology methods were characterized for properties, morphology, cytotoxicity and cell uptake. CV brain-targeting potential was evaluated in vitro on the hCMEC/D3 BBB-model, and in vivo/ ex vivo. CV sizes were between 135-285 nm; ζ-potential was negative. The Dehydration Rehydration method conferred highest calcein loading and latency to CVs, compared to other methods. Increased calcein-leakage from CVs compared to liposomes, indicated their poor integrity, which was increased by pegylation. In vivo results confirmed lower liver uptake by PEG-CVs (compared to non-pegylated) proving that calcein integrity test is useful for prediction of CV-biodistribution, as used for liposomes. Cell-uptake of homologous-origin CVs was not always higher compared to that of non-homologous. Nevertheless, CVs from hCMEC/D3 demonstrated highest BBB permeability (in vitro), compared to OX-26 targeted liposomes, and brain localization (in vivo). CVs from hCMEC/D3 cells grown in different media demonstrated decreased interaction with brain cells and brain localization; significant differences in proteome of the two latter CV types were identified by proteomics, suggesting a potential methodology for identification of organotropism-determining CV-components.

Introduction

Liposomes are known for their applications as efficient drug carriers (Farjadian et al., 2019; Allen and Cullis 2013), and today several liposomal drug products are available for clinical use while others are undergoing clinical testing (Rosenblum et al., 2018; Akhter et al., 2018; Belfiore et al., 2018). The therapeutic advantages of all liposomal drugs currently available in the clinic (compared to corresponding free drugs), are attributed to their modified pharmacokinetics; indeed, although active targeting of liposomes is under extensive exploration for more than 30 years, no ligand-targeted liposome (or other nanoparticle) product has been realized up-to-date, posing the most persistent bottleneck in drug delivery.

Recent knowledge about extracellular vesicles in regards to their intercellular communication pathways and their specific organotropic behavior has opened new and exciting horizons (Kooijmans et al., 2012; Van Dommelen et al., 2012; Aryani and Denecke, 2016). Besides local cell-to-cell communication (Meldolesi 2018; Maia et al., 2018) exosomes play key roles in interactions between cells located far apart from each other (Hoshino et al., 2015; Becker et al., 2016; Fu et al., 2016; Peinado et al., 2017). The tremendously high organotropism of specific exosome types is in fact the major unmet goal in the ligand-targeted-liposome field (Rosenblum et al., 2018). The complementarily of these two systems has currently initiated a novel fast-growing research field of *extracellular vesicles for drug delivery*. This field involves the design of targeted drug carriers, after identifying the key elements that dictate the biological fate of extracellular vesicles, and more specifically their ability to preferably interact with specific cells (Antimisiaris et al., 2018; Johnsen et al., 2014; Vader et al., 2016). However, one of the limitations towards rapid evolution and translation of exosomes into therapeutic products is the highly cumbersome and low-yield methodology for their isolation (Zheringer et al., 2015; Heinemann et al., 2014). To overcome the later drawback, the use of whole cells was proposed as an alternative. In fact, cellular vesicles (CVs) are reported to possess several advantages compared to exosomes, the main being their significantly higher production yield (Yoon et al., 2015; Jang et al., 2013; Lunavat et al., 2016; Goh et al., 2017a; & b; Jo et al., 2014; Wu et al., 2018).

Nevertheless, several key-points that will potentially contribute and accelerate CV exploitation towards development of more efficient targeted (artificial or biological) nano-carriers, are currently unresolved. In the current study we aimed to explore the following points:

(i) The particular **role of parental cells used for CV isolation on their potential to facilitate delivery of their contents into cells** (compared to liposomes). Although numerous studies have reported significantly higher cell uptake of CV- or exosome-associated drugs, compared to liposome-associated ones, it is not clear if CVs derived from specific parent cells will always demonstrate increased interaction towards the same cells compared to other cell types.

(ii) **The potential to load CVs with drugs by applying the DRV technique**, a method that achieves high loading of sensitive materials into liposomes (Antimisiaris, 2017), but was never tested for exosomes or CV loading.

(iii) The **utility of the calcein-latency method for evaluation of CV integrity**. This method provides important information about liposome integrity during their incubation in any media (Kokkona et al., 2000), and could perhaps serve the same purpose for CVs, acting as a useful tool for prediction of their *in vivo* fate.

(iv) The **potential of brain endothelial cell derived CVs to target the brain** (Poller et al., 2008), compared to CVs from other cells and targeted liposomes (Johnsen, et al., 2018).

To this end, we constructed CVs from three cell types; B16F10, HEK-293 and hCMEC/D3 cells, and explored the points mentioned above.

Materials and Methods

1,2-distearoyl-sn-glycerol-3-phosphatidylcholine (PC), 1,2-distearoyl-sn-glycero-3-phospho-(1'-rac-glycerol) (sodium salt) (PG) and 1,2-distearoyl-sn-glycerol-3-phosphoethanolamine-N-[methoxy(polyethyleneglycol)-2000] (PEG), 1,2-distearoyl-sn-glycero-3-phosphoethanolamine-N-[maleimide(polyethylene glycol)-2000] (PEG-MAL) and lissamine rhodamine B phosphatidylethanolamine (RHO) were purchased from Avanti Polar Lipids (Alabaster, AL. USA) . Cholesterol (99%) (Chol), Triton X-100, Calcein, Fluorescein-isothiocyanate-dextran-4000 (FITC), calcein, Lucifer yellow-CH dilithium salt (LY), and Sephadex G-50 were from Sigma-Aldrich (Darmstadt, DE). Lipophilic tracer, 1,1-dioctadecyl-3,3,3,3-tetramethylindotricarbocyanine iodide (DiR), used as lipid-label in CVs for live animal imaging, was form Molecular Probes (Eugene, OR, USA). Mouse anti-rat CD71 IgG2a (clone OX-26) was obtained from Serotec (Kidlington, UK). Protein concentrations were measured, by Bradford micro assay (Biorad, Hercules, CA, USA). All other chemicals were of analytical quality and were purchased from Sigma-Aldrich or Merck.

Fluorescence intensity (FI) of samples, was measured by a Shimatzu RF-1501 spectrofluoremeter (Shimatzu, Kyoto, JP), using EX-540/EM-590 nm for RHO detection, or EX-490 nm/EM-525 nm for FITC or calcein detection; in all cases 5 nm slits were used. A bath sonicator (Branson, Thermo Fisher Scientific, Waltham, MA, USA) and microtip-probe sonicator (Sonics and Materials, Leics, UK) were used for liposome and for CV preparation.

Preparation of Liposomes

Liposomes (LIP) composed of PC/Chol (2/1 mol/mol) and PC/PG/Chol (8.5/1.5/5 mol/mol), and pegylated liposomes (PEG-LIP) composed of PC/PG/Chol/PEG (7.9/1.5/5/0.6 mol/mol) were prepared by the thin film hydration method (Markoutsa et al., 2014). The thin lipid film was hydrated with PBS pH 7.40, or FITC-dextran (36mM) or calcein (100mM; osmolarity was adjusted to 300mOsm). After initial formation of the liposome dispersions, their size was reduced by probe sonication (Sonics & Materials). Free FITC-dextran or calcein was separated from liposomes by ultracentrifugation (40 min at 40.000 rpm, Sorvall WX90 Ultra, Thermo Scientific). Targeted

liposomes (t-LIP) were also prepared, consisting of PC/Chol/PEG /PEG-MAL (20:10:1.6: 0.04

mol/mol). Anti-transferrin monoclonal antibody OX-26 (at 0.1mol% density (compared to lipid))

attachment was performed by MAL-thioether reaction, as described in detail before (Markoutsa et al.,

2014). In brief, PEG-MAL containing LIPs were mixed with thiolated –OX-26 and incubated at room

temperature for 4 h, and then at 4°C overnight. Non-attached antibody was removed by gel filtration

(Sepharose 4B-CL) and the yield of Mab attachment was calculated by and Elisa technique as

described before (Markoutsa et al., 2014), and found to be 74% of the added amount of Mab, in

agreement with previous reported yields (Markoytsa et al., 2014; Papadia et al., 2017).

Cell Culture and CV formation

Three types of cells were used in this study: (i) Human HEK-293 embryonic kidney cells (HEK)

(American Type Culture Collection, VA) ; (ii) C57BL/6 mouse B16F10 skin melanoma cells (B16)

(National Cancer Institute Tumour Repository, Frederick, MD); And (iii) Immortalized human

cerebral microvascular endothelial cells (hCMEC/D3) (passage 25–35) which were obtained under

license from Institut National de la Sante et de la Recherche Medicale (INSERM, Paris, FR).

HEK and B16 cells were grown in RPMI 1640 medium supplemented with 10% FBS and 1%

antibiotic-antimycotic solution (Invitrogen, Carlsbad, CA, USA). The cells were cultured at 37°C, 5%

CO_2/saturated humidity. Medium was changed every 2–3 days.

hCMEC/D3 cells were grown in EndoGro medium (Merck, Darmstadt, DE) supplemented with 10

mM HEPES, 1 ng/ml basic FGF (bFGF), 1.4 uM hydrocortisone, 5 μg/ml ascorbic acid, penicillin-

streptomycin, chemically defined lipid concentrate, and 5% ultralow IgG FBS. In some cases the

hCMEC/D3 cells were grown in RPMI (as mentioned above). All cultureware were coated with 0.1

mg/ml rat tail collagen type I (BD biosciences, Franklin Lakes, NJ, USA

CVs were derived from hCMEC/D3, or HEK or B16 cells, cultured as mentioned above. In some

studies, CVs were isolated for hCMEC/D3 cells grown in RPMI instead of EndoGro. Cells were

incubated in T175 flasks until confluency, detached from flasks with trypsin, and washed thrice with

ice-cold PBS. Dispersions were probe sonicated (Sonics & Materials, Leics, UK), for up to 1min, and

CVs were isolated by ultracentrifugation (Thermo Sorvall WX90 Ultra, Thermo Scientific, Waltham, MA, USA) at 60.000 rpm for 2h at 4^0C and carefully re-suspended (in order to break aggregates) in PBS, pH 7.40.

In some cases, CVs were enriched with Chol and coated with PEG. For Chol enrichment, CVs (dispersed in H_2O) were incubated with Chol (10% w/w) at 37^oC for 30 min, followed by sonication (3 min) and subsequent exchange of H_2O with PBS (Zhang et al., 2017; Ying et al., 2018). CVs were then pegylated by incubation with PEG micelles (which were prepared by formation of a thin film of PEG, hydration with PBS, and incubation at 65^oC for 30min), for 2 h at 60^oC and then overnight at 4^oC (Kooijmans et al., 2016). PEG was used at a 10mol% (compared to CV lipid content).

CVs and liposomes were loaded with hydrophilic fluorescent dyes, for evaluation of CV loading efficiency (EE%) and integrity (calcein,100mM in PBS), and vesicle/cell interaction (FITC, 36mM in PBS). CV and liposome phospholipid content of was quantified by a method routinely used for measurement of liposomal lipid concentration (Stewart 2018); protein content of CVs was quantified by Bradford assay.

Size Distribution and Zeta Potential Measurements

The particle size distribution (mean hydrodynamic diameter and polydispersity index) of CVs and liposomes in 10mM PBS, pH 7.4 (at 0.4 mg/ml lipid) was measured by dynamic light scattering (DLS) (Malvern Nano-Zs, Malvern Instruments, Malvern, UK) at 25°C and a 173° angle. Zeta Potential was measured in the same dispersions, at 25°C, utilizing the Doppler electrophoresis technique.

Transmission Electron Microscopy (TEM)

CVs (0.5-1 mg/ml) were re-suspended in 10mM HEPES (to eliminate potential artifacts from phosphate) and then negatively stained with different staining solutions such as 2% ammonium molybdate and 1% neutral phosphotungstic acid (PTA), washed twice with dH_2O, drained with a tip of a tissue paper and observed at 100.000 eV with JEOL (JEM-2100) TEM (Jeol, Tokyo, JP) (Franken et al., 2017).

Methods for loading of CVs with hydrophilic dyes

CVs were initially extruded through polycarbonate filters with decreasing pore diameters, starting from 1000nm, 400nm and finally 100nm, and then divided in 1 mL parts, to apply different methods for calcein encapsulation, as described below:

Incubation Method: CVs were incubated at 37°C for 1 h with 1 mL calcein solution (100mM), applying vortex every 15 min.

Sonication Method: Calcein solution was mixed with CVs and the mixture was probe sonicated (at 28% intensity) 4 times for 30sec each time (2 min intervals).

Freeze thaw Method: 1 mL of calcein (100mM) was mixed with CVs. 10 cycles of freezing (30min at -80°C) and thawing (RT) were carried out.

DRV Method: CVs (suspended in 1 mL H_2O) and 1ml of calcein (100mM) was mixed, freeze-dried and rehydrated with dH_2O and PBS, as reported (Markoutsa et al., 2011).

After each loading method, CVs remained at room temperature for 1hr (to anneal any structural defects) and were then extruded through 100nm polycarbonate filters, in order to compare vesicles of the same size for loading efficiency. Non-associated calcein was separated from CVs by size exclusion chromatography (Sephadex G-50, Sigma-Aldrich, Darmstadt,DE) column (1x35 cm), eluted with PBS, pH 7.40. Fluorescence intensity (FI) of CV-loaded calcein was measured (EX 470 nm-EM520nm), after disruption of vesicles with Triton X-100. Calcein loading was calculated on the basis of a calibration curve (calcein concentration/FI).

Cytotoxicity Assay

Cytotoxicity assays were performed in order to evaluate whether CVs exacerbated toxicity to cells, under the conditions applying in the cell culture studies (concentration, incubation time). Cells were seeded and grown until confluent. Medium was replaced and CVs (6, 12 and 24nmoles [of lipid] per $3x10^4$ cells), LIP or PEG-LIP (at the same lipid concentration) were incubated with cells for 4 h at 37 °C, (5% CO_2/saturated humidity). Cell number was measured with a hemocytometer; 24 h incubations were also performed, in some cases. After incubation, medium was removed and cells were washed with PBS. Fresh medium containing 0.5 mg/ml 3-(4,5-Dimethylthiazol-2-yl)-2,5-diphenyltetrazolium

bromide (MTT) was added. Cells were incubated for 2 h, the medium was removed, and DMSO was added (at 37 °C for 30 min) to dissolve the formazan crystals that formed. Viable cells (%) were calculated based on the formula (A570sample - A570background)/(A570control -A570background) x 100, where A570control is the OD-570 nm of untreated cells and A570background the OD-570 nm of MTT without cells.

CV Integrity (in vitro)

The integrity of calcein-loaded CVs was studied by measuring the latency of CV-entrapped calcein, during incubation in absence/presence of serum proteins (80% FCS v/v) for 24h at 37°C. Liposomes were also studied under identical conditions for comparison. Calcein latency (percent) was calculated as previously reported (Kokkona et al., 2000).

Cell Uptake Studies

For evaluation of uptake of CV-entrapped drugs by cells, FITC-labeled CVs , LIPs and PEG-LIPs were incubated with confluent monolayer's of HEK, B16 and hCMEC/D3 cells (200 or 400nmoles liposomal or CV lipid/10^6 cells) in medium (containing 10% FBS (v/v)) at 37°C, for 4 h. Cells were then washed twice with ice-cold PBS, detached from plates by scraping, re-suspended in 1ml of PBS and assayed for FI (EX-490 nm/EM-525 nm, slits 5 nm), after cell lysis in 2% Triton X-100. Cell auto-fluorescence was always subtracted. In some cases, cell-uptake experiments were also done in medium containing 20% (v/v) FCS, to investigate the effect of increased serum protein levels on cell/CV interactions (Markoutsa et al., 2014). Sample protein content was measured by Bradford assay, and FITC uptake was normalized to protein concentration.

Flow Cytometry

FITC-labelled CVs derived from B16 and hCMEC/D3 cells were prepared as mentioned above (both, hCMEC/D3$_{EndoGro}$ and hCMEC/D3$_{RPMI}$ were used for CV isolation), and their uptake by cells was evaluated after incubation of 200nmole lipid with 10^6 cells for 4h. Flow cytometry was performed on a BD FACS Calibur flow cytometer (Becton Dickinson, Franklin Lakes, NJ, USA). At least 20,000 events were acquired. FITC positive cells were identified and their median fluorescent intensity (MFI) was estimated using FlowJo V10 software (Tree Star Inc., Ashland, OR, USA).

Confocal Fluorescence Microscopy

Cells were grown on collagen-covered coverslips and incubated with FITC (aqueous phase label) and RHO (membrane label) labeled CVs for 4h. Cells then were fixed in 4% paraformaldehyde for 10 min, stained with Hoechst for 5min and mounted on microscopy slides with Mowiol. Slides were observed using fluorescence microscopy on a SP5 confocal microscope (Leica, Heidelberg, Germany) to visualize their subcellular distribution.

Cell-monolayer permeation studies

hCMEC/D3 cells were seeded on type I collagen pre-coated Transwell filters (polycarbonate 6-well, pore size 0.4um; Millipore Merck, Darmstadt, DE) at 5×10^4 cells/cm^2. Assay medium was changed every 4 days, and transport assays were performed 10–12 days after seeding. 24h before each transport experiment, the medium was replaced with fresh medium containing 1nM simvastatin. For confirmation of cell junction formation, monolayers were periodically inspected by microscope and by trans-endothelial electrical resistance (TEER) monitoring with Millicell ERS-2 Epithelial VoltOhm meter (Millipore Merck, Darmstadt, DE). Monolayer quality was verified by measuring permeability of a highly hydrophilic, low molecular weight compound, lucifer yellow (LY); current values were then compared with reported ones (Poller et al., 2008; Markoutsa et al., 2011). Transport experiments were conducted in HBSS supplemented with 10mM HEPES and 1mM sodium puryvate in the cell culture medium. Transport was estimated by placing FITC-labeled CVs on the upper side of monolayer (200nmole lipid per well) and measuring FITC FI in the lower side at various time periods (10, 20, 30, 60, 90 and 120 min). Lucifer yellow (LY) was also added in each well and its permeability was calculated, to verify that vesicles did not modify the barrier. Control liposomes (LIP) and targeted liposomes (t-LIP), were also evaluated, for comparison.

Proteomic analysis

The biological replica of the vesicles generated from hCMEC/D3 cells cultured in RPMI medium or in EndoGro medium were incubated in 1 ml water in order to burst followed by dialysis and ultracentrifugation (2x 100 000xg). The pellet was lysed in 4% SDS / 0.1 M DTT at 98 C, incubated for 30 min in a sonicating water bath and subjected to Sp3 mediated Tryptic/LysC digestion according to the standard protocol (Hughes et al., 2019).

For LC-MS/MS, supernatant containing peptides was collected, dried down, reconstituted in 2% (v/v) ACN and 0.1% (v/v) formic acid, and incubated for 3 min in a sonication water bath. Peptide concentration was determined by Nanodrop absorbance at 280 nm. 3ug peptides were pre-concentrated with a flow of 3 ul/min for 10 min using a C18 trap column (Acclaim PepMap100, 100μm x 2cm, Thermo Scientific) and then loaded onto a heated at 35°C C18 column (50 cm,75 μm ID, particle size 2 μm, 100Å, Acclaim PepMap100 RSLC, Thermo Scientific). The binary pumps of the HPLC (RSLCnano, Thermo Scientific) consisted of Solution A (2% (v/v) ACN in 0.1% (v/v) formic acid) and Solution B (80% (v/v) ACN in 0.1% (v/v) formic acid). Peptides were separated using a linear gradient of 4% B up to 40% B in 210 min (flow rate 300nl/min). Eluted peptides were ionized by a nanospray source and detected by an LTQ Orbitrap XL mass spectrometer (Thermo Fisher Scientific, Waltham, MA, USA) operating in data dependent mode. Full scan MS spectra were acquired in the orbitrap (m/z 300–1600) in profile mode with the resolution set to 60,000 at m/z 400 and automatic gain control target at 106 ions. The six most intense ions were sequentially isolated for collision-induced (CID) MS/MS fragmentation and detection in the linear ion trap. Dynamic exclusion was set to 1 min and activated for 90 sec. Ions with single charge states were excluded. Lockmass of m/z 445,120025 was used for continuous internal calibration. XCalibur (Thermo Scientific) was used to control the system and acquire the raw files.

For protein identification/quantification, the mass spectral files (.RAW files) were processed using MaxQuant software (1.6.3.3) (Cox et al., 2008; ibid, 2014). Default parameters were used for protein identification and quantification. Trypsin specificity with two missed cleavages were allowed was set and minimum peptide length was set to 7 amino acids. Cysteine carbamidomethylation was set as fixed, and methionine oxidation, deamidation of asparagine and glutamine and N-terminal acetylation were set as variable modifications (maximum of 5 modifications per peptide). The false discovery rate both for peptide and protein were set to 1%. For calculation of protein abundances, label-free quantification (LFQ) was performed with both "second peptide" and "match between run" options enabled. The complete human database was downloaded from Uniprot (94731 entries, 05_11_18).

In vivo Studies - Biofluorescence Imaging

In vivo live animal imaging experiments were carried out, for estimation of pharmacokinetics and ex-vivo organ distribution of CVs. DiR-labelled-CVs were used, since free DiR is rapidly eliminated from mice following injection, as previously verified (Markoutsa et al., 2014; Papadia et al., 2017). CVs from hCMEC/D3 cells (grown in RPMI and EndoGro) and B16 cells were evaluated, as well as CVs that were enriched with Chol and PEG (as described above).

FVB (Friend leukemia virus B) albino mice and C57BL/6 mice, purchased from Hellenic Pasteur Institute (Athens, Greece) were bred at the Center for Animal Models of Disease, University of Patras, Faculty of Medicine (Rio, Greece). FVB mice were chosen for their white skin and fur that permits enhanced light penetration, while C57BL/6 mice were used as syngeneic to the B16-derived CVs. Animal care and experimental procedures were approved by the Veterinary Administration Bureau of the Prefecture of Achaia, Greece, protocol approval numbers 3741/16.11.2010, 60291/3035/19.03.2012, and 118018/578/30.04.2014), and were conducted according to Directive 2010/63/EU

(http://eurex.europa.eu/LexUriServ/LexUriServ.do?uri=OJ:L:2010:276:0033:0079:EN:PDF).and European Union Directive 86/609/EEC for animal experiments. Mice were sex-(male-female), weight- (20–25 g), and age- (6–12 weeks) matched. Biofluorescence imaging of living mice and explanted murine organs was done on an IVIS Lumina II imager (Perkin Elmer, Santa Clara, CA). Mice were anesthetized using isoflurane and serially imaged at various time-points, post-injection of DiR-labeled CVs (200μg lipid/mouse). Retro-orbital venous sinus injection, which is equally effective to tail-vein injection, was used, in order to avoid potential animal distress and/or retention of significant amounts of dose in the tail. Standard excitation/emission wavelengths for DiR, excitation: 710–760 nm; emission: 810–875 nm, were applied, and images were acquired and analyzed using Living Image v4.2 software (Perkin Elmer, Santa Clara, CA). In detail, bodily area- or explanted organ specific regions of interest were created and were superimposed over all images acquired in a uniform fashion; photon flux within these regions were measured.

Statistical Analysis

All results are expressed as mean ± SD from at least four independent experiments. Most data were analyzed by using one-way ANOVA followed by Bonferroni post hoc test. Statistical significance for all comparisons was set at p= 0.05. When more factors were compared two-way ANOVA was performed. The significance of comparisons is presented on the graphs.

For the Proteomic analysis results, statistical analysis was performed using Perseus (version 1.6.2.2) (Tyanova and Cox 2018). Proteins identified as "contaminants", "reverse" and "only identified by site" and with "less than 2 peptides identified" were filtered out. The LFQ intensities were transformed to logarithmic. Zero intensities were imputed (replaced by normal distribution). The replicas were grouped for each set of conditions, i.e. "RPMI medium" and "EndoGro Medium" a two-sided Student's t-test of the grouped proteins was performed using p values for truncation (p<0.05).

Results

Role of parental cells of CVs on their potential to facilitate delivery of their contents into cells

TEM studies revealed round-shape morphology of CVs (Fig.1.A). CVs prepared by processing HEK and B16 cells, had mean hydrodynamic diameters between 276 and 286 nm, more than 2 times higher than the 100nm membranes, from which they were extruded as the final step of their preparation procedure. Oppositely, the liposomes which were formulated by the same methodology had mean diameters close to 100nm; PDI values of CVs were also much larger compared to those measured for the liposomes (Table 1). The zeta-potential of the CVs was similar to that of the negatively charged (PC/PG/Chol) liposomes, in accordance to previous reports (Jung et al., 2013; Lunavat et al., 2016). CVs from HEK and B16 cells were loaded with FITC (by the DRV method), in order to evaluate their potential to facilitate delivery of their contents into cells; three liposome types with different lipid compositions were tested in parallel, for comparison. CVs and liposomes were initially demonstrated to be non-cytotoxic towards the cells under the conditions applying in the cell uptake study, as seen in Fig. 1.B and Fig. 1.C. Cell uptake study results show that B16 cells take up CVs_{HEK} at larger amounts compared to the (homologous origin) CVs_{B16}, at both doses used, 200nmoles (Fig.1.D) and 400nmoles (Fig. 1.E), indicating that CVs do not always demonstrate increased interaction with homologous (parental) cells, compared to vesicles from non-homologous origin. When the results of the two sets of experiments are compared (Fig. 1.D and Fig. 1.E), it is observed that while the uptake of CVs_{B16} by both cell types is saturated at the higher dose (%uptake values are lower at the higher dose), this is not the case for the CVs_{HEK}, indicating different uptake mechanisms of the two CV types; furthermore, CV uptake by B16 cells is higher than that by HEK cells for both CVs irrespective of the amount of CV-lipid incubated with the cells (200 or 400 nmole). Interestingly, the uptake of FITC by both cell-types is substantially higher (from 9 to 23 times) from the CVs, compared to all the liposome types evaluated (Fig 1.E). Considering the uptake of the liposomes by the cells (seen in Fig 1.F in magnification), most liposome-types are taken up at higher amounts by B16 cells compared to HEK cells (as observed also for CVs), with the exception of the negatively charged liposomes

(PC/PG/Chol). Also, PEGylated liposomes are seen to interact less with the cells, compared to the non-PEGylated liposome types.

Potential to load CVs with drugs by applying the DRV technique

The DRV method was never evaluated up-to-date for the loading of CVs or extracellular vesicles with aqueous soluble compounds, so we compared it with three other commonly applied methods, incubation, sonication and freeze-thawing method. Calcein-loaded CVs_{B16} prepared by the DRV method were found to have between 2 and 2.8 times higher calcein content (7% loading efficiency) compared to the CVs loaded with the other techniques (Fig 2.A). The lowest loading (2.49 %) was achieved by incubation, while sonication and freeze-thawing methods resulted in similar loading (3.28 % and 3.45 %, respectively), 30% higher compared to incubation.

Calcein-latency method for evaluation of CV integrity

Initial calcein latency values measured immediately upon dilution of the CVs (from B16 cells) in buffer, range between 14% - 52% (Fig 2.B) (irrespectively of the loading method used), which are very low compared to the usual values reported for liposomes composed of phospholipids and Chol (usually > 85%) (Kokkona et al., 2000; Markoutsa et al., 2011; ibid 2014), indicating poor vesicle integrity. Nevertheless, the CVs prepared by DRV method have the highest initial calcein latency values compared to those prepared by other methods (3 - 3.3 times lower latency values).

The release of CV-encapsulated calcein from vesicles was followed during 24h incubation in buffer, and as seen in Fig 2.C, calcein is gradually released from all CVs within the time period monitored. Concerning the size and polydispersity of the vesicles produced by the four different methods, we observe that all had similar mean diameters (between 135-153nm) and PDIs (from 0.22-0.29) (Fig, 2.D and 2.E.); for all CVs, size and PDI are stable after 3 days of storage at $4^{o}C$.

The conclusion from the above studies is that the DRV method produces CVs with substantially increased amounts of vesicle-associated calcein, a higher fraction of which is retained into the aqueous compartment of the vesicle upon dilution, compared to the vesicles produced by other

methods evaluated. Nevertheless, all CV-types released their calcein content after 24 h incubation in buffer.

The integrity of CVs prepared by DRV method from other cells (HEK and hCMEC/D3) was additionally studied, to confirm that the previous finding are not specific for CVs$_{B16}$. Initial calcein latency values of CVs$_{HEK}$ are similar to those of CVs$_{B16}$; while corresponding values of CVs$_{hCMEC/D3}$ are much lower (approx. half) (Table 2). No significant difference was observed between the different CVs considering their lipid/protein (w/w) ratios (Table 2).

The kinetics of calcein release from all CV types during 24h incubation in buffer and FCS, are seen in Fig 3. In all cases (Fig 3A-3C) calcein release is higher when CVs are incubated in buffer compared to FCS, which is not the case for liposomes (Fig.3.D). Additionally, all CVs tested, gradually release most of their calcein content during the 24h incubation period, confirming that this is not the case for CVs$_{B16}$ only. Furthermore, the substantial difference between the CVs and liposomes, in terms of their integrity is obvious, since initial calcein latency values for liposomes are between 86 and 94%. PEG-LIP demonstrate significantly high stability during the 24h incubation period studied (retaining >65% of the encapsulated calcein), whilst the non-PEGylated LIP gradually lose a significant amount of calcein during incubation in FCS; however, even non-PEGylated liposomes are very stable in buffer.

When CVs were engineered to increase their Chol content and to incorporate PEG in their membrane (as described in the methods section) their integrity, especially in FCS, was significantly increased ($p<0.05$), as demonstrated for PEG-CVsB16 (Fig 3.B) and PEG-CVs$_{hCMEC/D3}$ (Fig. 3.C). Additionally their initial calcein latency values (Table 2) were increased. The physicochemical properties of the vesicles are shown in Table 3.

Potential of CVs derived from brain endothelial cells to target the brain

CVs from the three different cell types used were studied for their interaction with hCMEC/D3 cellular model of BBB. Cell viability experiments verified that the CVs did not exhibit cytotoxic effects towards hCMEC D3 cells (Fig. 4.A), under the conditions applying in the studies. The cytotoxicity of some CV-types after 24 h incubation with B16 and hCMEC/D3 cells was additionally

18

evaluated, and the results show that cell viability is always slightly lower when the cells are incubated with CVs_{B16}, compared to $CVs_{hCMEC/D3}$; however CVs_{B16} had similar viability values to those of PEG-LIP which were also studied for comparison (*See Supplementary Data, Figure S1*).

The uptake of CV-associated FITC into the brain endothelial cells was calculated following CV/cell incubation, as a measure of the uptake of the CVs by the cells. Negative-charged liposomes (LIP) and also ligand-targeted liposomes (t-LIP), decorated with OX-26 monoclonal antibody against the transferrin receptor were also tested for comparison. The physicochemical properties of the vesicles used in this study are presented in Table 3. As seen in Fig 4.B, the uptake of $CVs_{hCMEC/D3}$ by the brain endothelial cells was several times higher compared to that of all the other CVs tested, as well as the conventional liposomes. In fact, compared to non-targeted LIP, all CVs demonstrated substantially higher uptake by hCMEC/D3 cells. Surprisingly, the uptake of $CVs_{hCMEC.D3}$ by the brain cells was also significantly higher compared to the uptake of the ligand-targeted liposomes (Fig.4.B). It is important at this point to mention that it was proven that the use of trypsin (as a cell detaching method) during $CVs_{hCMEC/D3}$ preparation did not decrease their uptake by hCMEC/D3 cells compared to CVs prepared without using trypsin (*See Supplementary Data, Figure S2*).

As seen in Fig. 4.C the uptake of $CVs_{hCMEC/D3}$ is slightly decreased when the experiment is carried out in presence of 20% (v/v) of serum (compared to 10%), while the corresponding differences for the other two CVs are not significant. When hCMEC/D3 cells are cultured in EndoGro medium they express specific proteins on their membranes which contribute to the formation of "tight" cell monolayers (Schrade et al., 2012). We sought to investigate if perhaps the CVs produced by the same cells grown in a different medium, such as RPMI, would demonstrate modulated cell interactions. Indeed, the uptake of $CVs_{hCMEC/D3}$ from cells grown in RPMI by hCMEC/D3 cells is approx. 2 times lower, compared to the uptake of $CVs_{hCMEC/D3}$ produced from cells grown in EndoGro (Fig. 4.D). A similar result was seen for the uptake of the same CVs by B16 cells (at a lower magnitude), while their uptake by the HEK cells was substantially modulated but in the opposite direction (CVs from cells grown in RPMI were taken up by HEK cells 2.5 times more, compared to CVs from cells grown in EndoGro). Thereby, it is indicated that the cell culturing conditions have significant effects on the interactions of the cell-derived CVs with different cells.

The CVs$_{hCMEC/D3}$ cell-uptake results were confirmed by flow cytometry (Fig.5.A) and confocal microscopy studies (Fig.5.B). Indeed, interaction of CVs$_{hCMEC/D3}$ produced by cells grown in EndoGro towards hCMEC/D3 cells was higher compared to CVs produced by cells grown in RPMI (Fig.5.A). Furthermore, the interaction of CVs$_{B16}$ with hCMEC/D3 cells was 3.0 – 4.7 times lower compared to the CVs$_{hCMEC/D3}$, in accordance with the results of the cell uptake experiment (Fig.4). Confocal microscopy confirmed that CVs (dually labeled with FITC (aqueous phase marker) and RHO (membrane marker)), are endocytosed in the cell cytoplasm (Fig.5.B). Confocal microscopy micrographs demonstrating quantitatively lower interactions (compared to Fig.5.B) between B16 cells and CVs$_{hCMEC/D3}$ or CVs$_{B16}$ can be seen in *Supplementary Data, Figure S3*.

TEM micrographs of CVs from hCMEC/D3 cells grown in the two different media (RPMI and EndoGro) prove that they have no morphological differences (*Supplementary Data, Figure S4*).

To explore the magnitude of the membrane composition differences between CVs$_{hCMEC/D3}$ produced by cells grown in the different media, proteomic analysis was performed. A total of 1460 confident protein groups were identified on CVs, and the statistical comparison of quantitative (LFQ) values for each protein in RPMI versus EndoGro culturing conditions gave a list of 171 proteins that were significantly altered as shown by a volcano plot in Figure 6 (see also *Supplementary Data, Table S1,* for the full protein list). These were analyzed by the protein subcellular annotation available at subcellbarcode.org (Orre et al., 2019), which revealed 28 proteins annotated to be localized as secretory and subcategorized into plasma membrane, ER, Mitochondrial, lysosomal, peroxisomal etc. (*Supplementary Data, Table S2).*

CVs$_{hCMEC/D3}$ were evaluated for their transport across the hCMEC/D3 cell monolayer model of the BBB. Plain negative-charge liposomes (PC/PG/Chol) (LIP) as well as ligand -targeted liposomes (t-LIP), were also evaluated for comparison. The TEER of the control monolayer (without any sample) was measured during monolayer formation and was found to gradually increase from 36 Ω cm^2 (at day 3) to 52.1 $\pm$ 2.4 Ω cm^2 and finally to 59.6$\pm$4.42 Ω cm^2 (after simvastatin treatment), and LY permeability was 1.04x10^{-3} $\pm$ 8.56x10^{-5}cm/min, all values being in good agreement with previously reported ones (Poller et al., 2008; Markoutsa et al., 2014). No significant differences were found in

the TEER and LY permeability values between all the monolayers used and the control (Table 4), proving that monolayer permeability was not affected by any of the samples. Concerning vesicle-associated FITC translocation across the monolayer, transport of $CVs_{hCMEC/D3}$ for the first 45 min was much higher compared to that of t-LIP, but after that, the transport rate of $CVs_{hCMEC/D3}$ was markedly decreased (Fig. 5.C). On the contrary t-LIP transport was initiated at a substantially lower rate, and gradually increased; finally the FITC amounts transported were similar to those from $CVs_{hCMEC/D3}$. As expected, the non-targeted liposomes were transported at a significantly lower degree, compared to both, t-LIP and $CVs_{hCMEC/D3}$. Permeability values are presented in Table 4. The values for LIP and t-LIP are in agreement with previously reported permeability values (Markoutsa et al., 2011; ibid, 2014).

In vivo Studies

I*n vivo* live-animal imaging, and ex vivo imaging of explanted organs, following injection of DiR-labeled $CVs_{hCMEC/D3}$ (in FVB mice) and CVs_{B16} (in syngeneic C57BL/6 mice), was used to explore CV pharmacokinetics and potential for brain targeting. Since the integrity of CVs was found to be low (as presented above), PEG-CVs were also studied. Physicochemical properties of vesicles used for in vivo studies are shown in Table 3. As seen in Figure 7, engineered CVs (for Chol and PEG incorporation) demonstrate lower distribution in the liver and localize in the brain at significantly higher amounts compared to the corresponding non-PEG vesicles. In fact the non-engineered CVs (depicted as CTR in the graphs) are rapidly accumulating in the liver and lung area as seen from the 15 min post-injection images (Fig. 7.A and Fig 7.D). The very fast accumulation of the DiR signal in liver and lungs indicates that CVs have low integrity and thus are most probably rapidly opsonized and cleared from circulation, having limited chances to distribute to other tissues. For both types of CVs (those from B16 and hCMEC/D3 cells) CV-engineering does not significantly modify the CV-associated signal in lungs; however PEG-CVs_{B16} have substantially lower signal in spleen compared to the corresponding control CVs. Oppositely DIR-signal in spleen is not significantly altered when the $CVs_{hCMEC/D3}$ are engineered.

In Fig 8.A the brain signal/Dose ratios measured 4h post-injection for the four different CV-types are compared. As seen the normalized DiR brain signal of PEG-$CVs_{hCMEC/D3}$ is highest followed by that of $CVs_{hCMEC/D3}$; the brain signals of CVs from B16 cells are lower, even those of the engineered CVs (although PEG-CV_{B16} brain signal is 3 times higher than the corresponding signal acquired by the non-engineered CVs_{B16}). In fact the different brain targeting potential between B16 cell and hCMEC/D3 cell derived CVs (especially since they were studied in different animal models), is better realized by comparison of the Brain/Liver+Spleen (DiR-signal) ratios (Fig.8.B), which is a more accurate measure of brain targeting capability. These ex vivo results are in good correlation with the in vitro hCMEC/D3 uptake results (Fig. 4.B).

In another in vivo study, two sets of CVs were evaluated; CVs from cells grown in RPMI (CVs_{RPMI}) and CVs from cell grown in EndoGro (CVs_{ENDO}). The kinetics of CV-associated DiR for both CV types studied was disappointing, since a very rapid uptake of the CVs by liver, lungs, and spleen is evident, as soon as 15 min post-injection (*Supplementary Data, Fig. S5*); thereby the potential of the CVs to target the brain could not be verified *in vivo*. The *ex vivo* bio fluorescence values, measured 4h post-injection, prove the high accumulation of the CVs in liver, lungs and spleen (*Supplementary Data, Fig. S5.C*), and also show that both CV types evaluated (those derived from cells grown in RPMI and those from EndoGro grown cells), seem to have slight difference in regards to their biodistribution; The decay of biofluorescence signals with time is demonstrated in the ex-vivo imaging of organs from two mice that received CV_{RPMI} and were harvested 4 h and 24h post-injection, respectively (*Supplementary Data, Fig. S5.A*); the decay in signals of all organs is obvious, with the exception of spleen, where the signal was increased at 24h compared to 4h. The very fast accumulation of the DiR signal in liver and lungs indicates that these natural CVs have low integrity (as indeed proven by the calcein latency study) and as a consequence, they are probably rapidly opsonized and cleared from circulation. However, when the ex-vivo brain signal measured 4h post-injection of the two CV-types are compared after being normalized to the total DiR-signal injected (dose), it is obvious that the CVs_{ENDO} are localized at higher amounts in the brain compared to CVs_{RPMI} (Fig 8.C).

Discussion

The current study provides new insights in the CVs for drug delivery field. First of all, concerning the **role of parental cells on CV potential to facilitate delivery into cells**, it was clearly demonstrated that homologous origin CVs do not always display increased interaction with parent cells, since CVs from HEK cells were taken up more by B16 cells, compared to CVs of homologous origin (Fig. 1.D).

Regarding the **potential to load CVs with drugs by the DRV technique**, it was proven that this well-known in liposome field method, can be applied for loading hydrophilic compounds into CVs. CV-loading achieved by DRV method was more than double compared to sonication, incubation and freeze-thaw cycles (Fig. 2.A), the methods commonly used (Antimisiaris et al., 2108). Interestingly, the loading method was also observed to influence the initial calcein latency of CVs, and the DRV method was found to be superior not only because larger amounts of calcein were loaded, but also because a higher fraction of the load was retained in vesicles (Fig 2.B and 2.C).

Nevertheless, the CV loading values conferred by the DRV method are lower, compared to those reported for liposomes (between 9-30%) (Fatouros et al., 2001; Mourtas et al., 2015). The later result is connected with the low initial calcein latency values of CVs (Table 2). Low initial calcein latency may be attributed to rapid "re-organization" of vesicles immediately upon dilution, as demonstrated for liposomes composed of plain DMPC (Kokkona et al., 2000), for "elastic vesicles" with no Chol in their membrane (Ntimenou et al., 2012), and when liposomes are diluted in membrane-disrupting media (Mourtas et al., 2008). The fact that some CV-types were found to have higher mean diameters, compared to the membrane-pores they were extruded through (Table 1), agrees with the possibility of high elasticity due to (possible) low cholesterol content (Ntimenou et al., 2012). Initial calcein latency values of CVs from hCMEC/D3 cells were substantially lower compared to those from B16 and HEK (Table 2), indicating that CV integrity is determined not only by the method used for preparation/loading, but also by the parent cell type.

Another possible explanation for the low initial calcein latency of CVs is that a high percent of "liposome-associated" calcein is "adsorbed" on vesicle surface, rather than "entrapped" in vesicles, which is relevant with the high protein content of CVs.

23

The **utility of calcein-latency method for evaluation of CV integrity** was confirmed. Calcein latency is routinely used as a method to monitor liposome integrity during incubation in various media, and predict blood circulation time. It has the advantage of measuring vesicle-encapsulated-calcein leakage at real time without separation from encapsulated dye. The integrity of CVs during incubation in buffer and FCS, as monitored by calcein latency, was found to be lower compared to liposomes (Fig 3), while liposome integrity was in agreement with previous reports (Kokkona et al., 2000; Mourtas et al., 2008). Since we did not carry out lipidomic analysis of the current CVs, we cannot be sure about the reason for their low integrity. Increased fractions of Chol in exosomes compared to cellular membranes were reported before (Llorente et al. 2013), and the higher rigidity of extracellular vesicles compared to cells was attributed to higher sphingomyelin, di-saturated lipid, and cholesterol contents (Huang et al. 2013, Ridder et al. 2014). However, little is known about CV rigidity/integrity. Recently, in order to load doxorubicin into CVs, it was necessary to enrich then with cholesterol (Zhang et al., 2017); the same was required for drug loading into platelet-derived CVs (Ying et al., 2018).

Furthermore, although there are some studies about *in vivo* therapeutic effects of CV-associated drugs, not much is known about their *in vivo* kinetics. Jang et al. performed numerous experiments with doxorubicin-loaded exosomes and CVs following injection in mice, and high accumulation of vesicle-associated dye in liver, lung and spleen was found 12h post-injection. However, nothing was mentioned about the circulation time of vesicles, or their tissue distribution at shorter periods. Despite limited knowledge about CV *in vivo* kinetics, several studies demonstrate rapid accumulation of exosomes in liver, spleen and lung; Smyth *et al.,* 2015, studied the kinetics of several exosomes types and found that the vast majority of injected unmodified-exosomes are cleared by RES before reaching tumors. Elsewhere, pegylation significantly increased the circulation half-life of exosomes (Kooijmans et al., 2016).

When the current CVs were engineered for Chol and PEG incorporation in their membranes, they demonstrated increased integrity according to the calcein integrity study (Fig.3). Based on the poor integrity of the non-engineered CVs, we would predict a short blood-circulation period and a rapid

24

accumulation in RES, upon in vivo injection; accordingly, slower accumulation in liver and higher

distribution in other organs would be expected for engineered CV-types. Indeed, in vivo and ex-vivo

studies, in which engineered and non-engineered CVs were compared (Fig. 7 and Fig. 8.A), confirm

the calcein-integrity-based predictions, proving the value of this in vitro test. Furthermore, our results

agree with the previous studies mentioned above.

In regards to the **potential of brain endothelial cell derived CVs to target the brain**, the high

uptake of $CVs_{hCMEC/D3}$ by the BBB model compared to other CV-types evaluated, as verified by FACS

and confocal microscopy (Fig 4, Fig 5), as well as their rapid/high transport across thee monolayer

BBB model (Fig. 5.C), prove that they have high potential for brain targeting. In fact, this is the first

study that proves higher BBB targeting potential of CVs, compared to OX-26 liposomes. Since

recognition of targeting ligands on nanoparticles may be blocked after adsorption of serum proteins

on their surface (Salvati et al., 2013), it was proposed that vesicle/cell interaction studies in presence

of increased protein concentrations, may provide insights about the former possibility (Markoutsa et

al., 2014). The interaction of $CVs_{hCMEC/D3}$ with BBB cell was slightly decreased when cell-medium

protein concentration was increased (Fig. 4), suggesting a possibility for such "blocking" effects.

Coating of CVs-surface with PEG may -in addition to providing increase integrity- also help in this

direction. The results of the in vivo studies (Figs 7 and 8) clearly demonstrate higher brain targeting

potential of $CVs_{hCMEC/D3}$, compared to CVs_{B16}, in accordance to previous reports (Weskler et al.,

2005; Yang et al., 2015; Chen et al., 2016). The difference between the two CV-types in respect to

their brain targeting potential is better realized when the Brain/Liver+Spleen (DiR-signal) ratios

(Fig.8.B), are compared. Furthermore, although the unmodified $CVs_{hCMEC/D3}$ did not demonstrate

exceptionally high brain targeting potential (most probably due to low circulation time and rapid

uptake by liver and spleen), it was realized that engineering methods (similar to those used in

liposome technology) could increase the integrity of natural CVs, in order for the latter to exhibit their

high organotropism after systemic administration. Comparison of the 4h post-injection

Brain/Liver+Spleen DiR signal ratios of the current $CVs_{hCMEC/D3}$ ($4.90 \pm .83$) and especially the PEG-

$CVs_{hCMEC/D3}$ (12.1 ± 1.6), with reported ratios of BBB-targeted liposomes (with one and two ligands)

(which range between 0.3 - 1.6, 8h post injection, and 0.6 – 1.5, 24h post-injection) (Markoutas et al., 2014; Papadia et al., 2017), reveal the enhanced potential of the current CVs as brain-targeted carriers for theragnostic agents.

The finding that culturing conditions (media) of parent cells may have such a significant effect on the targeting capability of the CVs, as demonstrated herein in vitro (Figs 4, and 5), and in vivo (Fig. 8.C) is very interesting, and may be used as a methodology to identify exosomal surface proteins (or protein combinations) which are important for targeting, facilitating the development of artificial exosome mimetics. Previously hCMEC/D3 exosomes were characterized for their signature profiles, and 1179 proteins were identified (Weskler et al., 2005), many of them similar to the 1460 protein groups currently identified in the CVs from the same cells.

Some of the surface proteins (highlighted in the volcano plot of Fig.6), such as PHB2, HSPA8, PDIA4, ITGA2, NT5E, EPHA2, HLA-C, PHB, HLA-B, AIMP1 and TLN1, may be interesting for further exploitation in order to assess if the observed differences could explain the deregulation in CV interaction with hCMEC/D3 cells. Interesting groups are proteins that share their involvement in cellular adherence (heat shock cognate 71 kDa protein, integrin alpha-2, ephrin type-A receptor 2 and talin-1) that might influence the vesicle-cellular junction-interaction. Additionally, proteins PHB and PHB2, although mitochondrial, might confer to the vesicle biology.

Acknowledgments

Authorship Contributions

Participated in research design: A. Marazioti, G.T.Stathopoulos, G. Panayotou, S.G Antimisiaris

Conducted experiments: A. Marazioti, K. Papadia, M. Kannavou, M. Spella, A. Basta, A-L de Lastic,

M. Rodi, M. Samiotaki,

Contributed new reagents or analytic tools: G. Panayotou, M. Samiotaki, A. Mouzaki, G.T.

Stathopoulos

Performed data analysis: A. Marazioti, K. Papadia, M. Samiotaki, S.G. Antimisiaris

Wrote or contributed to the writing of the manuscript: A. Marazioti, M. Samiotaki, A. Mouzaki, S.G.

Antimisiaris.

References

Akhter MH; Rizwanullah M; Ahmad J; Ahsan MJ; Mujtaba MA, and Amin S (2018) Nanocarriers in advanced drug targeting: Setting novel paradigm in cancer therapeutics. *Artif. Cells Nanomed. Biotechnol.* **46**:873–884.

Allen TM, and Cullis PR (2013) Liposomal drug delivery systems: From concept to clinical applications. *Adv. Drug Deliv. Rev* **65**: 36–48.

Antimisiaris SG (2017) Preparation of DRV liposomes, *Methods in Molecular Biology* **1522**: 23-47.

Antimisiaris SG, Mourtas S, and Marazioti A (2018) Exosomes and exosome-inspired vesicles for targeted drug delivery. *Pharmaceutics* **10**(4):218-

Aryani A, and Denecke B (2016) Exosomes as a Nanodelivery System: A Key to the Future of Neuromedicine? *Mol. Neurobiol* **53**: 818–834.

Becker A, Thakur BK, Weiss JM, Kim HS, Peinado H, and Lyden, D (2016) Extracellular vesicles in cancer: Cell-to-cell mediators of metastasis. *Cancer Cell* **30**:836–848.

Belfiore L, Saunders DN, Ranson M, Thurecht KJ, Storm G, and Vine KL (2018) Towards clinical translation of ligand-functionalized liposomes in targeted cancer therapy: Challenges and opportunities. *J. Control. Release* **277**:1–13.

Chen CC, Liu L, Ma F, Wong CW, Guo X, Chacko JV, Farhoodi HP, Zhang SX, Zimak J, Ségaliny A, Riazifar M, Pham V, Digman MA, Pone EJ, and Zhao W. (2016) Elucidation of Exosome Migration across the Blood-Brain Barrier Model In Vitro. *Cell Mol Bioeng* **9**(4): 509–529.

Cox J, and Mann M. (2008) MaxQuant enables high peptide identification rates, individualized p.p.b.-range mass accuracies and proteome-wide protein quantification. *Nat Biotechnol* **26**(12):1367-72.

Cox J, Hein MY, Luber CA, Paron I, Nagaraj N, and Mann M (2014) Accurate Proteome-wide Label-free Quantification by Delayed Normalization and Maximal Peptide Ratio Extraction, Termed MaxLFQ. *Mol Cell Proteomics* **13**(9): 2513–2526.

Farjadian F, Ghasemi A, Gohari O, (...), Karimi M, and Hamblin MR (2019) Nanopharmaceuticals and nanomedicines currently on the market: Challenges and opportunities, *Nanomedicine* **14**(1):93-126.

Fatouros DG, Hatzidimitriou K, and Antimisiaris SG (2001) Liposomes encapsulating prednisolone and prednisolone-cyclodextrin complexes: Comparison of membrane integrity and drug release, *Eur J Pharm Sciences* **13**(3):287-296.

Franken LE, Boekema EJ, and Stuart MCA (2017) Transmission Electron Microscopy as a Tool for the Characterization of Soft Materials: Application and Interpretation. *Adv. Sci.* **4**:1600476

Fu H, Yang H, Zhang X, and XuW (2016) The emerging roles of exosomes in tumor-stroma interaction. *J. Cancer Res. Clin. Oncol* **142**:1897–1907.

Goh WJ, Lee CK, Zou S, Woon EC, Czarny B, and Pastorin G (2017a) Doxorubicin-loaded cell-derived nanovesicles: An alternative targeted approach for anti-tumor therapy. *Int. J. Nanomed* **12**:2759–2767.

Goh WJ, Zhou S, Ong WY, Torta F, Alexandra AF, Schiffelers RM, Storm G, Wang JW, Czarny B, Pastorin G. (2017b) Bioinspired Cell-Derived Nanovesicles versus Exosomes as Drug Delivery Systems: A Cost-Effective Alternative. *Sci. Rep.* **7**:14322.

Heinemann ML, Ilmer M, Silva LP, Hawke DH, Recio A, Vorontsova MA, and Vykoukal J. (2014) Benchtop isolation and characterization of functional exosomes by sequential filtration. J. *Chromatogr. A* **1371**:125–135.

Hoshino A, Costa-Silva B, Shen TL, Rodrigues G, Hashimoto A, Tesic Mark M, Molina H, Kohsaka S, Di Giannatale A, Ceder S, et al. (2015) Tumour exosome integrins determine organotropic metastasis. *Nature* **527**:329–335

Huang X, Yuan T, Tschannen M, Sun Z, Jacob H, Du M, Liang M, Dittmar RL, Liu Y, Liang M, Kohli M, Thibodeau SN, Boardman L, and Wang L (2013) Characterization of human plasma-derived exosomal RNAs by deep sequencing. *BMC Genomics* **14**: 319.

Hughes CS, Moggridge S, Müller T, Sorensen PH, Morin GB, and Krijgsveld J (2019) Single-pot, solid-phase-enhanced sample preparation for proteomics experiments. *Nature Protocols* **14**: 68–85.

Jang SC, Kim OY, Yoon CM, Choi DS, Roh TY, Park J, Nilsson J, Lötvall J. Kim YK, and Gho YS. (2013) Bioinspired exosome-mimetic nanovesicles for targeted delivery of chemotherapeutics to malignant tumors. *ACS Nano* **7**:7698–7710

Jo W, Kim J, Yoon J, Jeong D, Cho S. Jeong H, Yoon YJ, Kim SC, Gho YS, and Park J. (2014) Large-scale generation of cell-derived nanovesicles. *Nanoscale* **6**:12056–12064

Johnsen KB, Gudbergsson JM, Skov MN, Pilgaard L, Moos T, and Duroux M (2014) A comprehensive overview of exosomes as drug delivery vehicles—Endogenous nanocarriers for targeted cancer therapy. *Biochim. Biophys. Acta* **1846**: 75–87

Kokona M, Kallinteri P, Fatouros D, and Antimisiaris SG. (2000) Stability of SUV liposomes in the presence of cholate salts and pancreatic lipases: Effect of lipid composition. *Eur. J. Pharm. Scienc* **9**:245-252.

Kooijmans SAA, Fliervoet LA, van der Meel R, Fens MH, Heijnen HF, van Bergen En Henegouwen PMP, Vader P, and Schiffelers RM (2016) PEGylated and targeted extracellular vesicles display enhanced cell specificity and circulation time. J. *Control. Release* **224**: 77–85.

Kooijmans SA, Vader P, van Dommelen SM, van Solinge WW, and Schiffelers RM, (2012) Exosome mimetics: A novel class of drug delivery systems. *Int. J. Nanomed* **7**:1525–1541.

Llorente A, Skotland T, Sylvänne T, Kauhanen D, Róg T, Orłowski A, Vattulainen I, Ekroos K, Sandvig K. (2013) Molecular lipidomics of exo-somes released by PC-3 prostate cancer cells. *Biochim Biophys Acta* **1831**: 1302–1309.

Lunavat TR, Jang SC, Nilsson L, Park HT, Repiska G, Lässer C, Nilsson JA, Gho YS, and Lötvall J (2016) RNAi delivery by exosome-mimetic nanovesicles—Implications for targeting c-Myc in cancer. *Biomaterials* **102**,:231–238.

Maia J, Caja S, Strano Moraes MC, Couto N, and Costa-Silva, B (2018) Exosome-Based Cell-Cell Communication in the Tumor Microenvironment. *Front. Cell Dev. Biol.* 6:18.

Markoutsa E, Pampalakis G, Niarakis A, Romero IA, Weksler B, Couraud P-O. et al,. (2011) Uptake and permeability studies of BBB-targeting immunoliposomes using the hCMEC/D3 cell line. *Eur J Pharmaceut Biopharmaceutics* **77**:265-274.

Markoutsa E, Papadia K, Giannou AD.et al., (2014). Mono and dually decorated nanoliposomes for brain targeting, in vitro and in vivo studies. *Pharm Res* **31**(5):1275-1289.

Meldolesi J. (2018) Exosomes and Ectosomes in Intercellular Communication. *Curr. Biol.* **28**:R435–R444.

Mourtas S, Diamanti G, Foka A, Spiliopoulou I, and Antimisiaris SG. (2015) Inhibition of bacterial attachment on surfaces by immobilization of tobramycin-loaded liposomes. *J Biomed Nanotechnology* **11**(12):2186-2196.

Mourtas S, Duraj S, Fotopoulou S, and Antimisiaris SG. (2008) Integrity of liposomes in presence of various formulation excipients, when dispersed in aqueous media and in hydrogels. *Colloids and Surfaces B: Biointerfaces* **61**(2):270-276.

Ntimenou V, Fahr A, and Antimisiaris SG. (2012) Elastic vesicles for transdermal drug delivery of hydrophilic drugs: A comparison of important physicochemical characteristics of different vesicle types. *J Biomed Nanotechnology* **8**(4):613-623.

Orre LM, Vesterlund M, Pan Y, Arslan T, Zhu Y, Fernandez Woodbridge A, Frings O, Fredlund E, and Lehtiö J. (2019) SubCellBarCode: Proteome-wide Mapping of Protein Localization and Relocalization. *Mol Cell* **73**(1):166-182.

Papadia K, Giannou AD, Markoutsa E, et al., (2017). Multifunctional LUV liposomes decorated for BBB and amyloid targeting - B. In vivo brain targeting potential in wild-type and APP/PS1 mice. *Eur. J. Pharm. Sciences* **102**:180-187.

Peinado H, Zhang H, Matei IR, Costa-Silva B, Hoshino A, Rodrigues G, Paila B, Kaplan RN, Bromberg JF, Kang Y et al. (2017) Pre-metastatic niches: Organ-specific homes for metastases. *Nat. Rev. Cancer* **17**:302–317.

Poller R, Gutman H, Krahenbuhl S, Weksler B, Romero I, Couraud PO, et al, (2008) The human brain endothelial cell line hCMEC/D3 as a human blood-brain barrier model for drug transport studies. *J Neurochem* **107**:1358–68.

Ridder K, Keller S, Dams M, Rupp AK, Schlaudraff J, Del Turco D, Starmann J, Macas J, Karpova D, Devraj K, Depboylu C, Landfried B, Arnold B, Plate KH, Höglinger G, Sültmann H, Altevogt P, and Momma S. (2014) Extracellular vesicle-mediated transfer of genetic information between the hematopoietic system and the brain in response to inflammation. *PLOS Biology* **12** :art. e1001874.

Rosenblum D, Joshi N, Tao W, Karp JM, and Peer D. (2018) Progress and challenges towards targeted delivery of cancer therapeutics. *Nat. Commun* **9**:1410.

Salvati A, Pitek AS, Monopoli MP, Prapainop K, Baldelli-Bombelli F, Hristov DR, Kelly PM, Åberg C, Mahon E, and Dawson KA, (2013) Transferrin-functionalized nanoparticles lose their targeting capabilities when a biomolecule corona adsorbs on the surface. *Nature Nanotech* **8**:137-143.

Schrade A, Sade H, Couraud P-O, Romero IA, Weksler BB, and Niewoehner J. (2012) Expression and localization of claudins-3 and -12 in transformed human brain endothelium. *Fluids and Barriers of the CNS* **9** :6.

Smyth T, Kullberg M, Malik N, Smith-Jones P, Graner M.W, and Anchordoquy TJ. (2015) Biodistribution and Delivery Efficiency of Unmodified Tumor-Derived Exosomes. *J. Control. Release* 199:145–155.

Stewart JCM, (1980) Colorimetric determination of phospholipids with ammonium ferrothiocyanate. *Anal Biochem* **104**:10-14.

Tyanova S, and Cox J. (2018) Perseus: A bioinformatics platform for integrative analysis of proteomics data in cancer research. *Methods Mol Biol.* **1711**:133–48.

Vader P, Mol EA, Pasterkamp G, and Schiffelers RM (2016) Extracellular vesicles for drug delivery. *Adv. Drug Deliv. Rev*. **106** Pt A:148–156.

Van Dommelen SM, Vader P, Lakhal S, Kooijmans SA, van Solinge WW. Wood MJ, Schiffelers, RM. (2012) Microvesicles and exosomes: Opportunities for cell-derived membrane vesicles in drug delivery. *J. Control. Release* **161**:635–644.

Wu JY, Ji AL, Wang ZX, Qiang GH, Qu Z, Wu JH, and Jiang CP (2018) Exosome-Mimetic Nanovesicles from Hepatocytes promote hepatocyte proliferation in vitro and liver regeneration in vivo. *Sci. Rep.* **8**:2471.

Yang T, Martin P, Fogarty B, Brown A, Schurman K, Phipps R, Yin VP, Lockman P, and Bai S. (2015) Exosome delivered anticancer drugs across the blood-brain barrier for brain cancer therapy in Danio rerio. *Pharm Res.* **32**(6):2003-14.

Ying M, Zhuang J, Wei X, Zhang X, Zhang X, Jiang Y, Dehaini D, Chen M, Gu S, Gao W, et al. (2018) Remote-Loaded Platelet Vesicles for Disease-Targeted Delivery of Therapeutics. *Adv. Funct. Mater.* **28**:1801032.

Yoon J, Jo W, Jeong D, Kim J, Jeong H, and Park, J. (2015) Generation of nanovesicles with sliced cellular membrane fragments for exogenous material delivery. *Biomaterials* **59**:12–20.

Zhang X, Angsantikul P, Ying M, Zhuang J, Zhang Q, Wei X, Jiang Y, Zhang Y, Dehaini D, Chen M. et al. (2017) Remote Loading of Small-Molecule Therapeutics into Cholesterol-Enriched Cell-Membrane-Derived Vesicles. *Angew. Chem. Int. Ed. Engl*. **56**:14075–14079.

Zheringer E, Barta T, Li M, and Vlassov A. (2015) Strategies for Isolation of Exosomes. *Cold Spring Harb. Protoc.* **2015**:319–323.

JPET # 257097

Footnotes

Conflicts of interest: All authors disclose no conflict of interest.

35

Legends for Figures

Figure 1. Results of preliminary studies: Representative negative stain TEM micrographs of CVsB16 (**A**) (with ammonium molybdate as stain [A1], or Phosphotungstic acid 1% [A2, A3]). Cytotoxicity of various concentrations of CVs from HEK and B16 cells, and three different liposome types (6, 12 and 24 nmoles of lipid/ 30000 cells), expressed as % Viability of control, after 4h co-incubation at 37 ^{o}C towards HEK cells (**B**) and B16 cells (**C**). Uptake of CV- or liposome- associated FITC, by B16 cells and HEK cells, following 4h incubation at 37 ^{o}C, of 200 nmoles lipid/10^6 cells (**D**) or 400 nmoles lipid/10^6 cells (**E**). The part of graph E which corresponds to the liposome formulation uptake is presented in magnified form (**F**). Significance of individual differences of CV/liposomes between the two cell types is presented as asterisks on the top of the bars, and other individual differences are presented by connecting lines. One-way ANOVA p-values (for the effect of CV-type) are shown.

Figure 2. A] Calcein encapsulation (expressed as calcein/lipid (mole/mole) Final/ C/L Initial) in CVsB16 using different loading methods. B] Initial Calcein latency values (%) in PBS (pH 7.40) of CVsB16 loaded with different methods. C] Integrity of CVsB16 during incubation in PBS (37°C, 24h). D & E] Mean hydrodynamic diameter and Polydispersity Index of CVsB16, immediately after preparation and after 3d. Each value is the mean value from four different preparations, and the bars represent the SD value of each mean. One-way ANOVA p-values for significant differences are shown on each graph.

Figure 3. Time course of Calcein Latency from CVs of various origin and liposomes (for comparison) during their incubation in PBS Buffer and FSC (80% v/v) for 24h (37°C) (mean values (n=4) ±SD). CV (or LIP) lipid concentration was 0.5mg/mL. **A]** CVs$_{HEK}$; **B]** CVs$_{B16}$ and PEG-CVs$_{B16}$; **C]** CVs$_{hCMEC/D3}$ and PEG- CVs$_{hCMEC/D3}$; **D]** PC/PG/Chol liposomes and PEG-LIP (PC/PG/Chol/PEG). Two-way ANOVA p values are reported on graphs for the effect of PEG.

Figure 4. A] Effect of CVs on viability of hCMEC/D3 cells, after incubation of various concentrations for 4 h. LIP (PC/PG/Chol) are also tested as controls. B] Uptake of various CV types and liposomes by hCMEC/D3 cells following 4h incubation of 200nmoles lipid/10^6 cells. C] Effect of

serum concentration of media on the interaction between CVs and hCMEC/D3 cells. D] Uptake of CVs$_{hCMEC/D3}$ by hCMEC/D3, B16 and HEK cells. The CVs were produced by cells grown in EndoGro or RPMI medium. Significance of individual differences is presented as asterisks on the top of the bars (or on connecting lines). Significant one-way (B) or two-way (C & D) ANOVA p-values are shown in the graphs.

Figure 5. [**A**] Flow cytometry interactions of various CVs (indicated in graphs) with hCMEC/D3 cells, shown in corresponding morphological plots; B] Representati laser-confocal micrograph (and magnification of indicated part) of hCMEC/D3 cells after interaction with CVs$_{hCMEC/D3}$. Cells for CV preparation were cultured in EndoGro. CVs were labelled with FITC (green, aqueous phase label) and RHO (red, membrane label); Hoeckst 33342 (blue) shows the nucleus; [**C**] Transport of vesicle-associated FITC across hCMEC/D3 cell monolayers (% of Total). Samples (200nmoles of each vesicle type) were added on transwell-mounted monolayers and transport was calculated by measuring FITC FI. Each result is the mean from 6 different experiments. Significance of individual differences is presented as asterisks (connecting lines indicate comparison). Two-way ANOVA p-values (for comparison of all cases (all), and comparison between CVs and t-LIP) are shown.

Figure 6. Volcano plot with the 171 proteins identified to be significantly altered between the two CV groups evaluated. The surface proteins that may be interesting to further evaluate are highlighted.

Figure 7. In vivo live animal- and ex-vivo imaging studies. In all cases CVs as well as corresponding PEG-CVs were tested under identical conditions to evaluate the effect of CV engineering on their in vivo fate. Representative images of mice after injection of 200ug lipid/mouse, 15 min and 4h post-injection (**A & D**); Ex vivo imaging of extracted organs 4 h post-injection (**B & E**); and graphs showing the comperative DiR signals of extracted organs (brain, liver, lung and spleen) from mice injected with non-pegylated CVs (CTR) vs PEG-CVs (PEG) (C&F). Figures A-C correspond to CVs$_{B16}$ injected in syngeneic C57BL/6 mice, and Figure D-F correspond to CVs$_{hCMEC/D3}$ injected in FVB mice. Each value is the mean from at least 6 animals.

Figure 8. A] Comparison of ex vivo DiR-signals (Photons/s) normalized to the total DiR-signal injected (dose), in brain of mice 4h post-injection of various types of CVs; FVB mice (for CVs$_{hCMEC/D3}$) and C57BL/6 mice (for CVs$_{B16}$) were used. **B**] Comparison of the 4h post-injection Brain/Liver+Spleen (B/L+S) DiR signal ratios of the same CVs as in A. **C**] Comparison of DiR-signals (Photons/s) normalized to the total DiR-signal injected (dose) in brain of FVB mice, 4h post-injection of CVs derived from hCMEC/D3 cells grown in EndoGro (ENDO), and in RPMI. All values are mean values from at least 4 or 6 animals.

Tables

Table 1. Physicochemical properties (Mean Diameter, polydispersity Index (PDI) and ζ-potential), of cellular vesicle from HEK (CVs $_{HEK}$) and B16 (CVs $_{B16}$) cells, and various liposome types (mean value (n=3 preparations) ± SD).

Vesicle type	Mean Diameter (nm)	PDI	ζ-potential (mV)
CVs $_{HEK}$	276.5 ± 8.0	0.423 ± 0.017	-12.3 ± 0.35
CVs $_{B16}$	285.9 ± 4.2	0.307 ± 0.018	-12.3 ± 0.42
PC/Chol LIP	125.3 ± 2.3	0.198 ±0.024	-2.27 ± 0.28
PC/PG/Chol LIP	116.6 ± 1.1	0.134 ±0.011	-15.2 ± 0.14
PEG LIP	123.6 ± 1.5	0.165 ±0.031	-1.90 ± 0.31

Table 2. Initial Calcein latency (%) in PBS and FCS, and Lipid/Protein (w/w) ratios of CVs from

different cells (mean (n= 5 preparations) ± SD).

Initial Calcein Latency (%)		Lipid/Protein (w/w)
FCS	**PBS**	
CVs_{B16}		
58.1 ± 9.2	44.9 ± 6.2	1.62 ± 0.20
CVs_{HEK}		
58.3 ± 7.5	42.9 ± 6.0	1.95 ± 0.27
$CVs_{hCMEC/D3}$		
31.7 ± 0.4	23.6 ± 1.6	1.87 ± 0.18
$PEG\text{-}CVs_{B16}$		
78.2 ± 2.8	64.9 ± 1.2	-
$PEG\text{-}CVs_{hCMEC/D3}$		
59.8 ± 1.5	37.9 ± 2.8	-

Table 3. Physicochemical properties of the vesicles used in calcein release, cell interaction (in vitro) and in vivo studies. Mean Diameter, polydispersity Index (PDI), and ζ-potential of CVs from HEK cells (CVs$_{HEK}$), B16 cells (CVs$_{B16}$) and hCMEC/D3 cells (CVs $_{hCMEC}$), as well as pegylated CVs$_{B16}$ ($_($PEG- CVs$_{B16}$) and pegylated CVs$_{hCMEC/D3}$ $_($PEG- CVs$_{hCMEC/D3}$). Liposomes (LIP), pegylated liposomes (PEG-LIP) (PC/PG/Chol/PEG) and targeted liposomes (t-LIP) properties are also reported.

Vesicle type	Mean Diameter (nm)	PDI	ζ-potential (mV)
LIP	126.6 ± 8.1	0.134±0.001	-15.1 ± 1.4
PEG-LIP	141.1 ± 1.1	0.169 ± 0.009	-3.40 ± 0.77
CVs $_{HEK}$	205 ± 49	0.375±0.018	-12.3 ± 0.42
CVs $_{B16}$	219 ± 1.8	0.322±0.032	-12.27 ± 0.42
PEG-CVs $_{B16}$	229.4 ± 9.4	0.318 ±0.083	-5.46 ± 0.56
CVs $_{hCMEC/D3}$	122.1 ± 6.7	0.255±0.013	-13.21 ± 0.43
PEG-CVs$_{hCMEC/D3}$	156.9 ± 4.3	0.335 ±0.117	-7.47 ± 0.29
t-LIP	180.9±17.54	0.241±0.051	-1.90 ± 0.31

Table 4. . Trans-endothelial resistance (TEER), LY-Permeability values (measured on the monolayers were the corresponding vesicle samples were placed), and FITC permeability values of the vesicle-associated FITC for the vesicle-types tested. Each value is the mean of 6 monolayer experiments from 2 different samples.

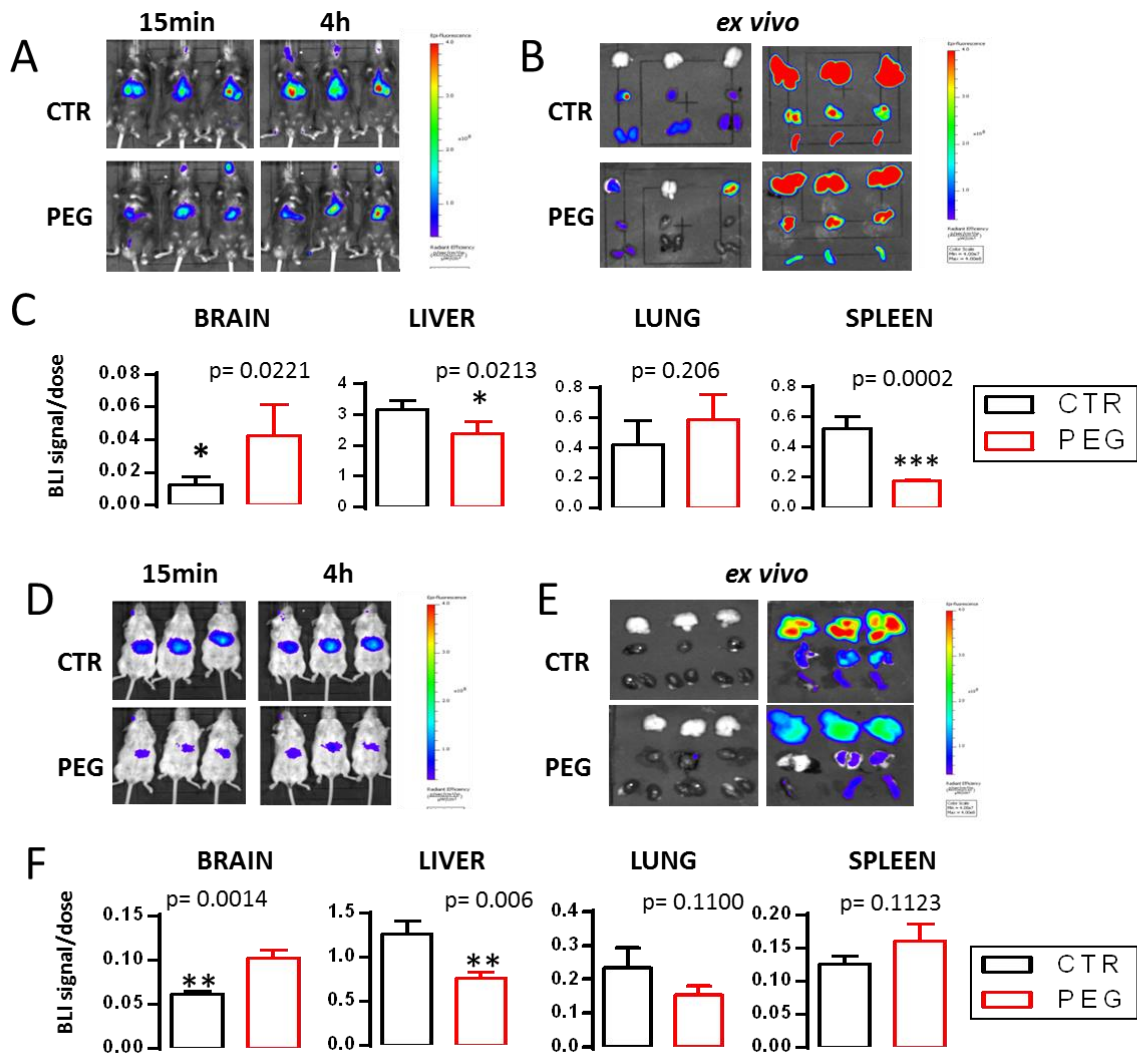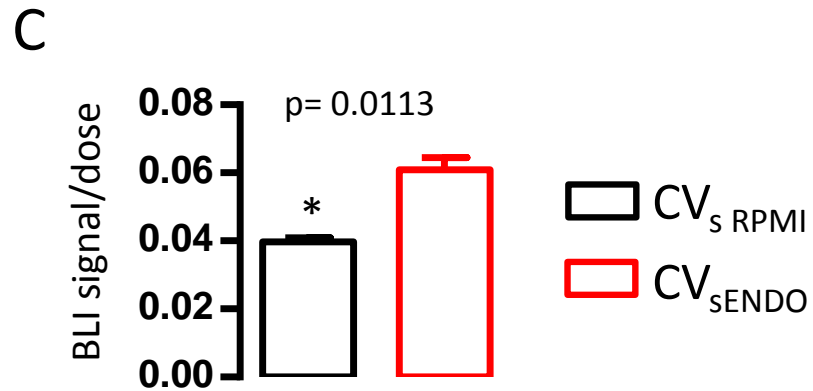| Vesicles	TEER ($\Omega*cm^2$)	LY Permeability (cm/min)	FITC Permeability (cm/min)
CVs $_{hCMEC/D3}$	56.7 ± 2.4	1.04E-03	1.3E-04 ± 2.5E-05
t-LIP	62.0 ± 5.3	1.06E-03	1.0E-04 ± 6.8E-06
LIP	58.8 ± 4.2	1.11E-03	2.6E-05±2.6E-06

Figures
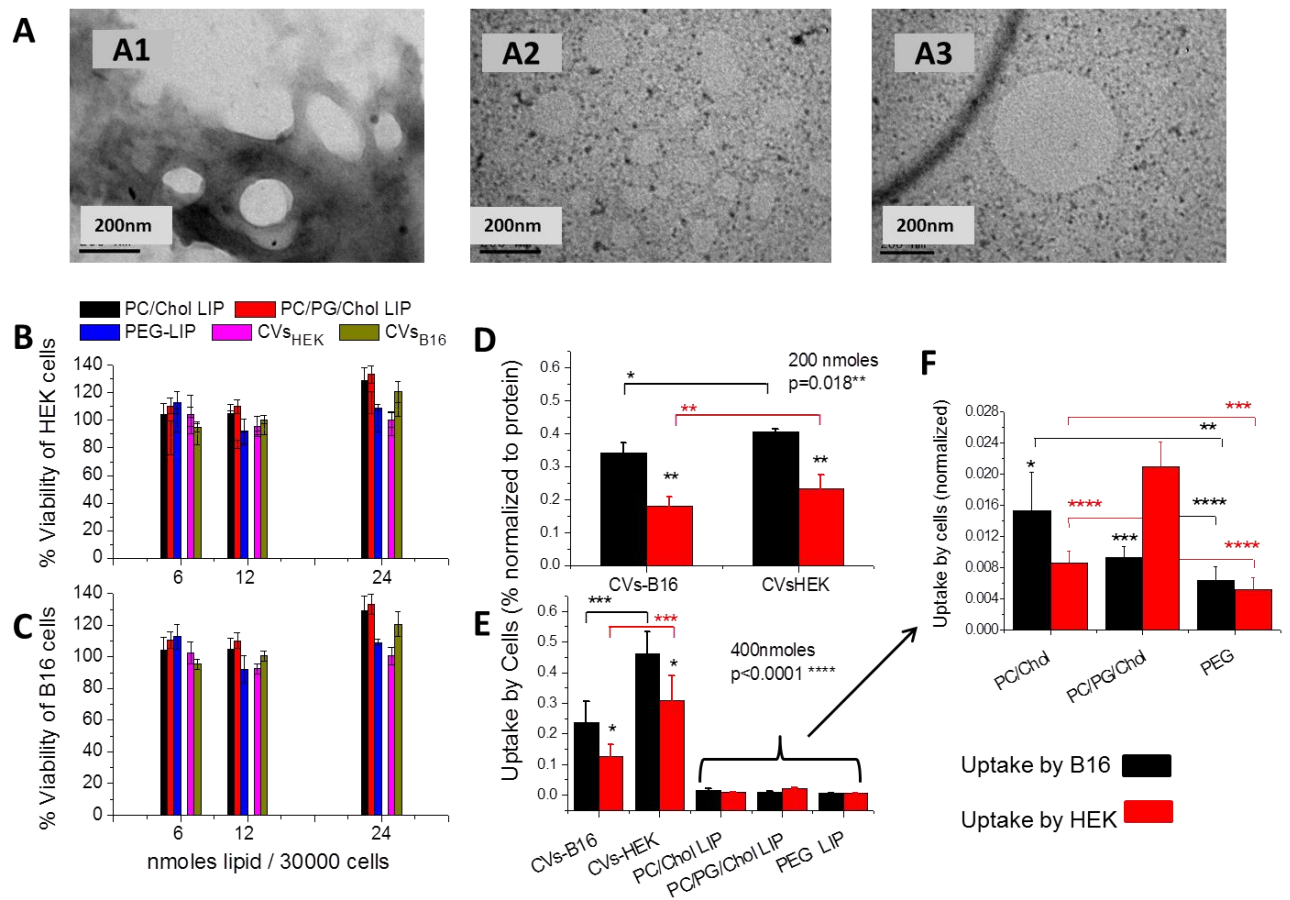
Figure 1
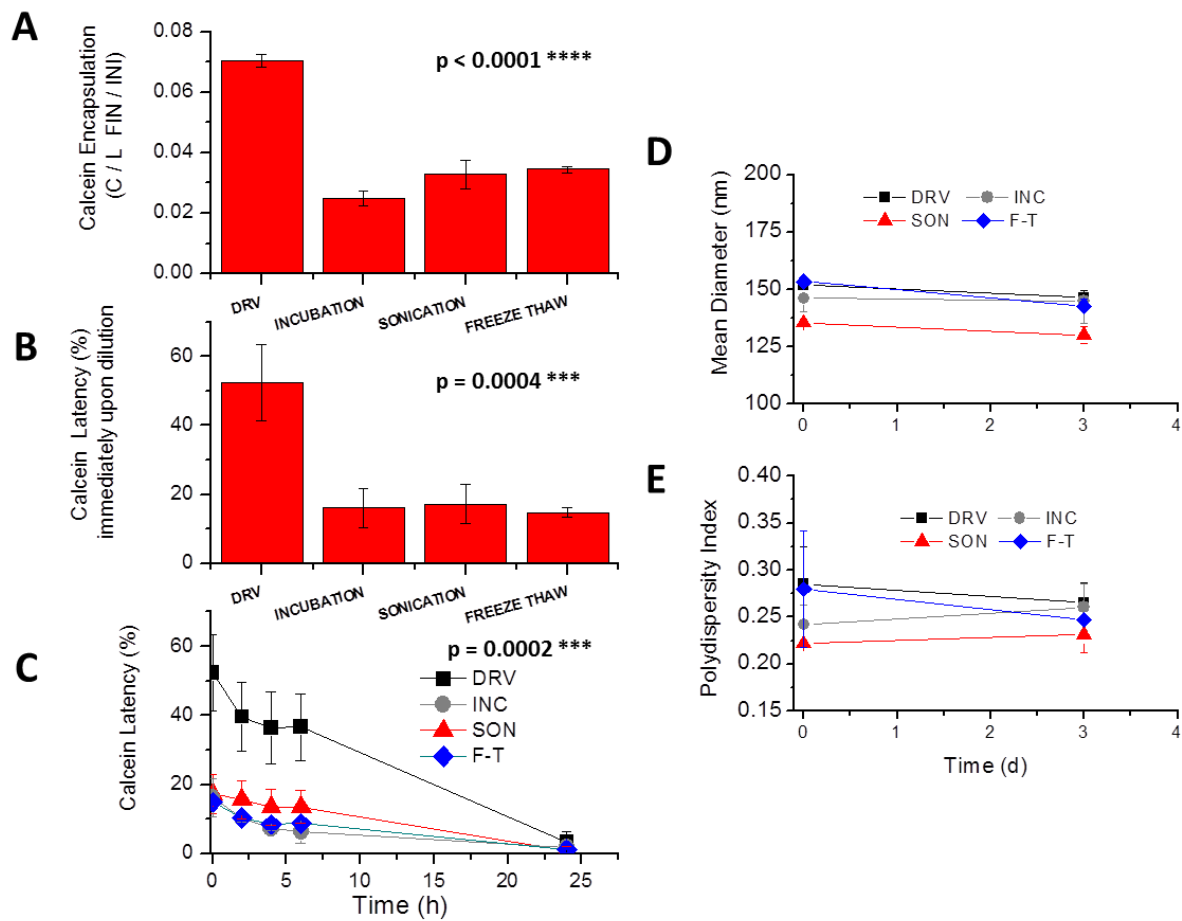
Figure 2
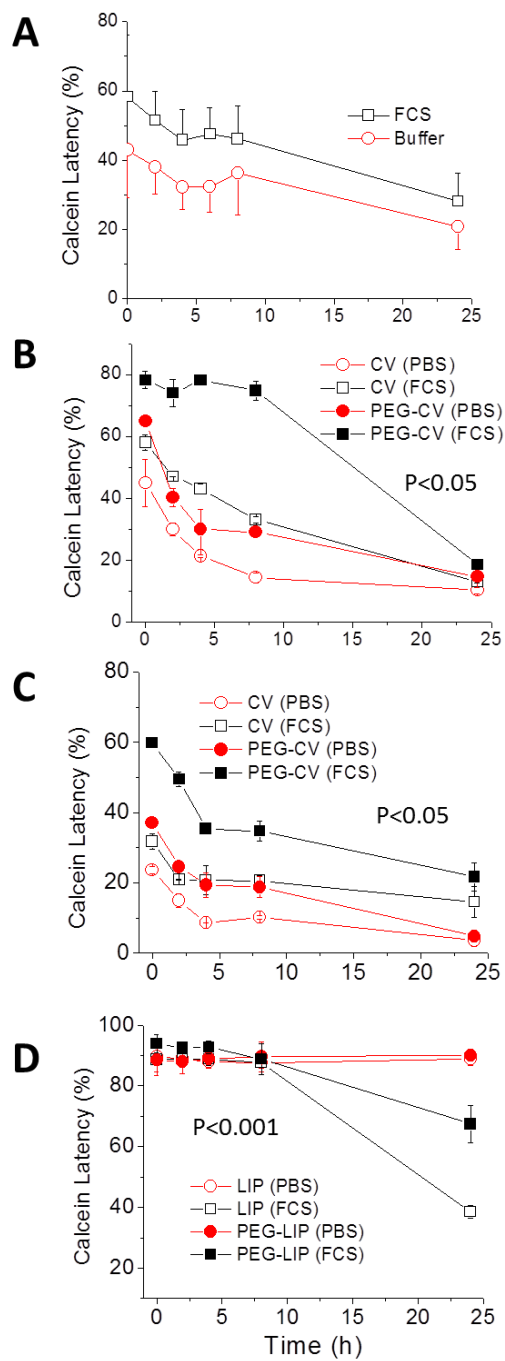
Figure 3
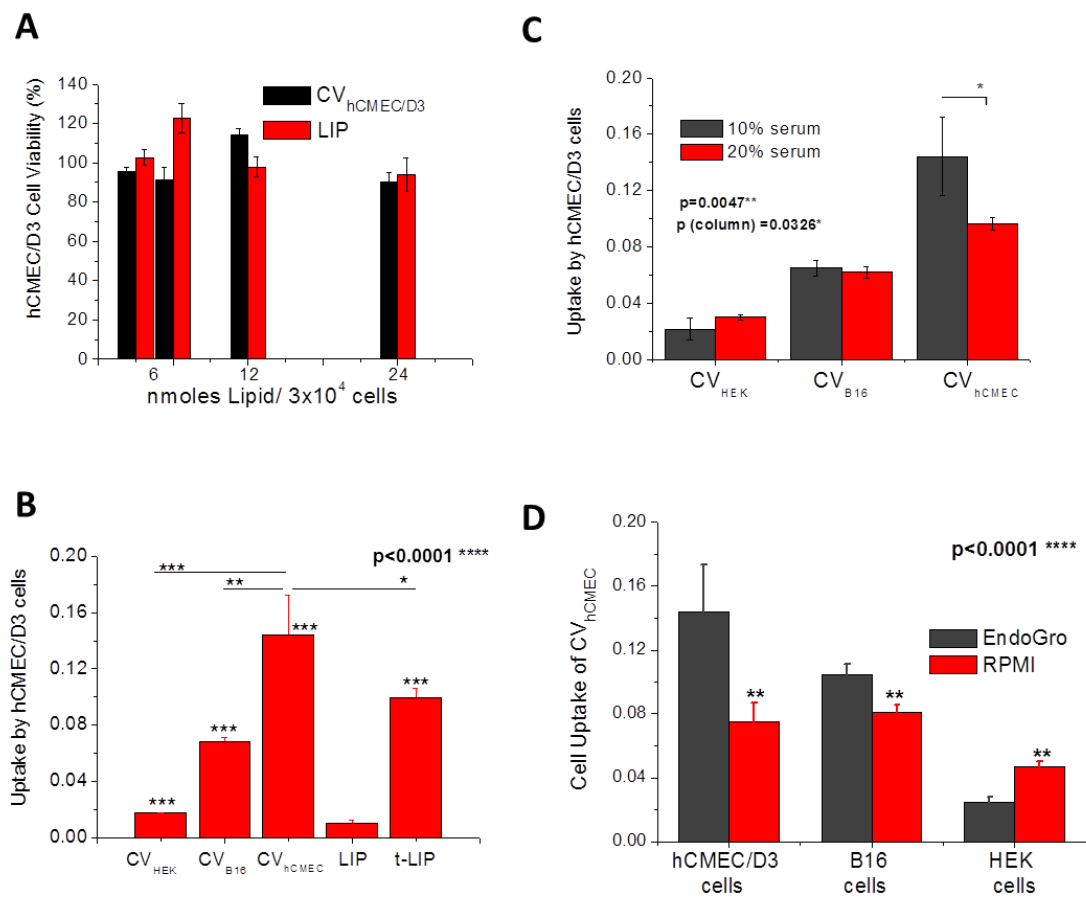
Figure 4
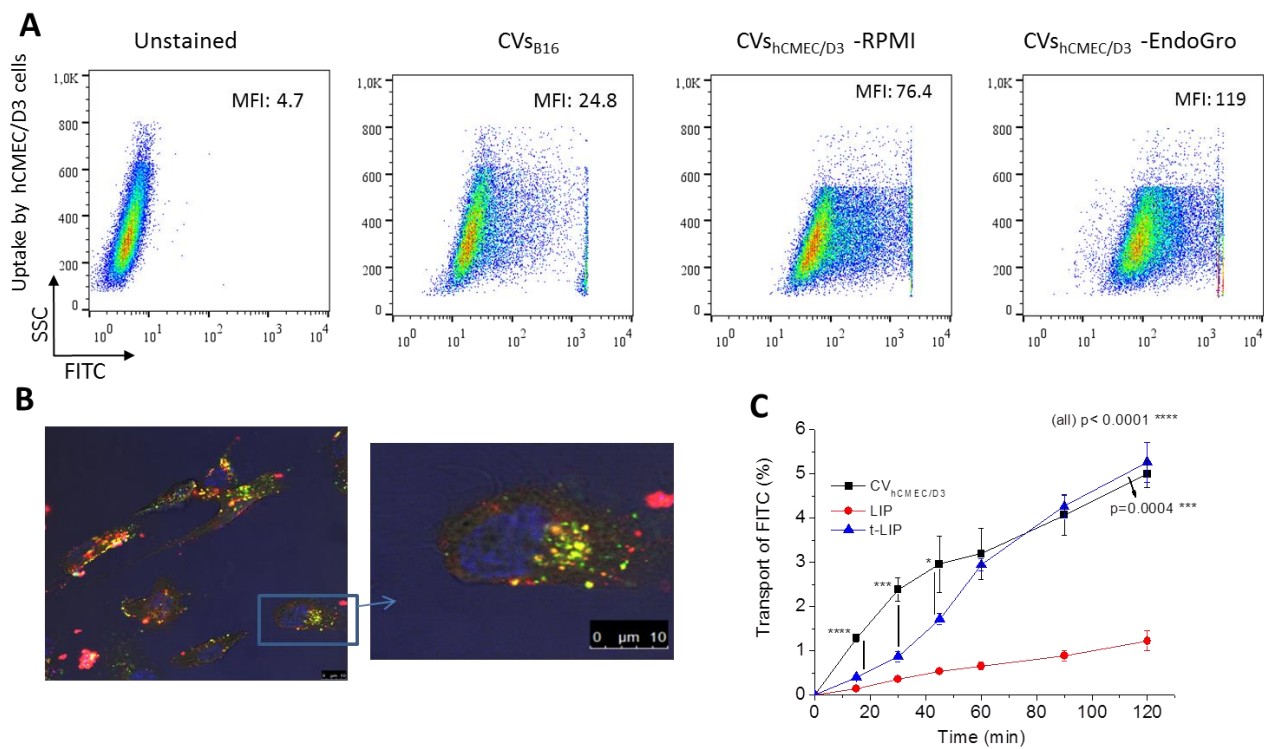
Figure 5
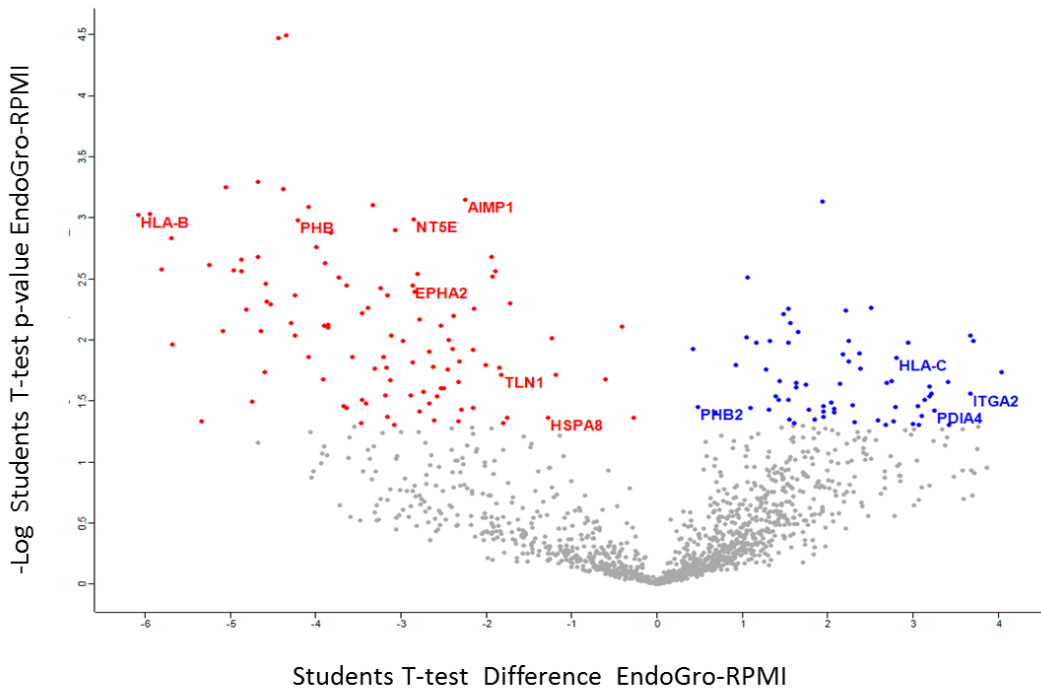
Figure 6

Figure 7

Figure 8